Band Gap Engineering of Mg Doped ZnO Nanorods Prepared by a Hydrothermal Method

*Sevim D. Senol, Cihat Boyraz, Ersin Ozugurlu, Ali Gungor, and Lutfi Arda**

The effect of band gap on the structure, magnetic, and optical properties of $Zn_{1-x}Mg_xO$ nanorods synthesized by hydrothermal method using varying x-values from 0.00 to 0.05 with 0.01 step increment is studied. The structural phases of $Zn_{1-x}Mg_xO$ samples are determined by X-ray diffraction tool. The Rietveld analysis is performed for the selected $Zn_{0.95}Mg_{0.05}O$ sample and all samples' phases are found as single phase. The concentration-dependent of lattice parameters, cell volumes, microstrain, and dislocation density, locality of the atoms and their displacement, and bond length in $Zn_{1-x}Mg_xO$ structures are detailed. Electron Spin Resonance (ESR) measurements are performed and analyzed through concentration dependence of the g-factor and the line-widths of pike to pike (ΔH_{PP}) of ESR spectra. A ferromagnetic behavior of the $Zn_{0.95}Mg_{0.05}O$ nanorods is observed. The optical band gaps (E_g) of $Zn_{1-x}Mg_xO$ nanorods are obtained by the data taken from Ultraviolet–Visible (UV–VIS) diffuse reflectance spectroscopy. It is found that the E_g-values increased with increasing amount of Mg elements in the structure.

1. Introduction

The zinc oxide (ZnO) nanostructure comes forward from among the II-VI semiconductors with very attractive properties such as the exciting binding energy of 60 meV at room temperature and a direct wide band gap of 3.37 eV. These properties have been used for the development of optoelectronic materials and applications.[1–11] Electro-optical and structural properties of ZnO nanomaterials can be controlled and improved by doping process with various elements. According to ref. [9] silver doping not only improves the absorption of the photocatalysts but also causes red-shift in the absorption band. Band gap reduction means that lower energy is required for the electron-hole pair generation. Another doping element lowering the band gap of ZnO is cerium which was studied by Sinha et al.[4] who revealed that cerium doping decreased size of nanorods, increased the intensity of green emission peak in photoluminescence, and decreased the band gap energy to 3.18 eV from 3.37 eV. Moreover, gallium-doped ZnO is also an important material due to its high carrier concentration and electrical conductivity, especially higher gallium doping produces a decrease of the band gap values of ZnO. Among these various doping elements, cadmium decreases to approximately 3 eV[5] and magnesium increases the band gap to 4 eV and higher.[2,11] In addition, magnesium doping might be suitable for enhancement of structural, electrical, and optical properties of ZnO. Moreover, the Mg^{2+} ions can also be successfully incorporated into the lattice of ZnO nanostructures due to its ionic radius (0.57Å) close to the ionic radius of Zn^{2+} (0.60Å).[12]

The wurtzite-type ZnMgO alloys have important applications in optoelectronic and display devices. Alloying of wurtzite ZnO with cubic MgO develops metastable wurtzite ($x < 0.5$) or zincblende ($x > 0.5$) crystals. Recent optical studies of ZnMgO indicated that with increasing Mg content the energies of the fundamental band-to-band transitions were found to be strongly blue shifted. Heiba and Arda[2] reported that magnesium content in ZnO must be high to achieve the true blindness and to extend the band gap energy. However, they found out that unstable phase mixing could occur because of the large crystal structure dissimilarity between wurtzite-hexagonal ZnO and rock-salt-cubic MgO.

Dr. S. D. Senol
Abant Izzet Baysal University
Faculty of Arts and Science
Department of Chemistry
14280 Bolu, Turkey

Dr. C. Boyraz
Marmara University
Faculty of Technology
Department of Mechanical Engineering
Goztepe, 34722 Istanbul, Turkey

Dr. E. Ozugurlu
Istanbul Technical University
Faculty of Science and Arts
Department of Mathematical Engineering
34467 Maslak, Istanbul, Turkey

Prof. A. Gungor
Bahcesehir University
Faculty of Medicine
Department of Biophysics
34734 Kadikoy, Istanbul, Turkey

Prof. L. Arda
Bahcesehir University
Faculty of Engineering and Natural Sciences
Department of Mechatronic Engineering
34349 Besiktas, Istanbul, Turkey
E-mail: lutfi.arda@eng.bau.edu.tr

The ORCID identification number(s) for the author(s) of this article can be found under https://doi.org/10.1002/crat.201800233

DOI: 10.1002/crat.201800233

Recently various techniques for the formation of Mg-doped ZnO nanostructures and films are reported in the literature; such as the microwave heating method,[13] auto combustion method,[14] pulsed laser deposition (PLD),[15] two-step method,[12] sol–gel method,[16] chemical vapor deposition (CVD),[12] and hydrothermal synthesis.[17–19] Among these, the popularity of the hydrothermal method is increasing day by day because of its efficient and tolerable growth condition, good potential for environmentally-safe production, suitability to any type of doping, easy control of dopant concentration, low cost with the use of water as a reaction medium, and mainly material synthesis for single crystal growth.[20,21]

In this study, we report different compositions of Mg-doped ZnO ($Zn_{1-x}Mg_xO$: $x = 0.0, 0.01, 0.02, 0.03, 0.04, 0.05$) nanorods synthesized by the hydrothermal method. Our aim is to figure out the effect of Mg doping on the structural, magnetic, and optical properties of ZnO nanorods using X-ray diffraction (XRD), Scanning Electron Microscopy (SEM), Energy-dispersive X-ray spectroscopy (EDS), and UV-visible diffuse reflectance spectroscopy techniques.

2. Experimental Section

Mg doped zinc oxide nanorods were synthesized at various concentrations ($Zn_{1-x}Mg_xO$: $x = 0.0, 0.01, 0.02, 0.03, 0.04, 0.05$) by hydrothermal method. Zinc nitrate (Zn(NO3)2, Alfa Aesar), magnesium acetate tetrahydrate, and hexamethylenetetramine (HMTA) were used as precursor materials. Deionized water was used as a solvent. 0.1 M aqueous precursor solution was prepared by dissolving Zn(NO3)2 and Mg in deionized water and stirring for an hour at room temperature. After dissolving the precursor, equal mole of hexamethylenetetramine was added to the solution and stirred for another one hour. After this step, 80 mL of prepared solution is transferred to 100 mL autoclaves. The reaction was conducted in an electric oven at 100 °C. After that, Mg doped ZnO nanoparticles were separated from the solution by using a centrifuge. Separated nanoparticles were washed with deionized water and dried in air.

Room temperature XRD measurements were performed for Mg doped ZnO nanorods by Rigaku Multiflex X-ray diffraction (XRD) instrument with monochromated Cu Kα (1.5418Å) source in the 2θ scan range of 20° to 80° and the scan speed 3 min^{-1} with 0.02 step increment. The surface morphologies of the samples were evaluated by Scanning Electron Microscopy (SEM-EDX) Jeol-6390-LV. The optical reflectance properties of the samples were carried out by Shimadzu 2600 Plus UV-Spectrophotometer with diffuse reflectance attachments. ESR spectra of $Zn_{1-x}Mg_xO$ (where $x = 0.0, 0.01, 0.02, 0.03, 0.04$, and 0.05) nanorods were collected at room temperature on a Bruker EMX model X-band spectrometer operating at a frequency of 9.8 GHz.

3. Results and Discussion

3.1. Structure Analysis

The structure of the all samples was determined by XRD analysis in the range of $20° \leq 2\theta \leq 80°$ degrees. The strongest peak was indexed as (100) for all dopant rates. The excessive magnesium contribution in especially $Zn_{0.95}Mg_{0.05}O$ revealed an increase in (002) peak intensity. All peak positions were indexed in **Figure 1**a and the secondary phase was not observed in all sample XRD patterns. The Rietveld refinement was exhibited for $Zn_{0.95}Mg_{0.05}O$ to present the sample quality in Figure 1b. Small variations which were found by the difference between observed and calculated were given by the blue color line in Figure 1b. This is an indication of a well-refined sample. The vertical pink colored bars depict Bragg reflection positions in the sample. Using the Debye Sherrer equation[21] and the full width at half maximum value (β), the average particle size (D) of $Zn_{1-x}Mg_xO$ samples were calculated and reported in **Table 1**. The nanorod's sizes of the samples are in fluctuation tendency with the increment of Mg elements in the stoichiometric samples and the contribution rate of $x = 0.05$ gives the lowest particle size (29.26 nm).

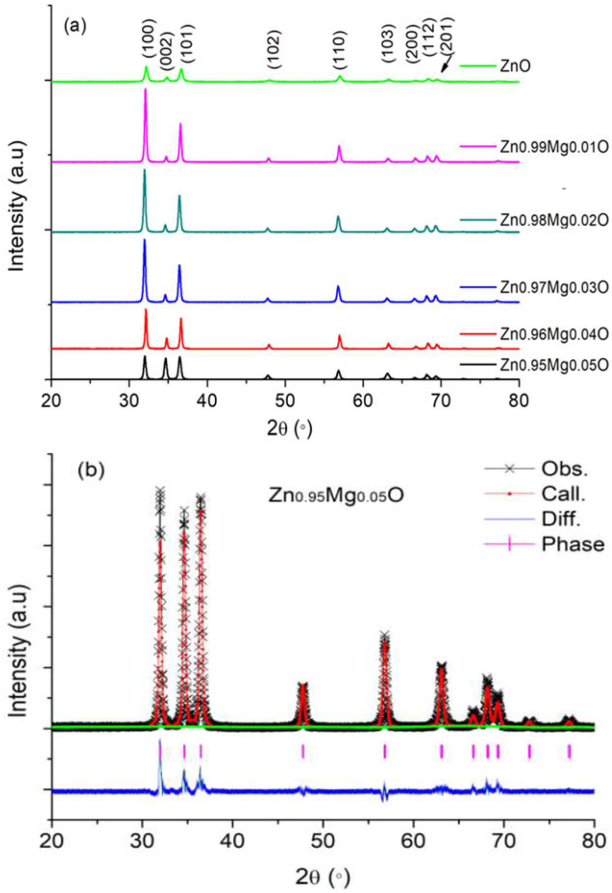

Figure 1. XRD analysis of all $Zn_{1-x}Mg_xO$ in a) and the Rietveld analysis of $Zn_{0.95}Mg_{0.05}O$ sample in b).

$$D = \frac{K\lambda}{\beta \mathrm{Cos}\theta} \tag{1}$$

In Equation (1), θ, K, and λ are the diffraction angle of the corresponding peak, 0.9 constant value, and 0.15406 nm X-ray wavelength, respectively. The lattice parameters (a and c) and cell volume variations of $Zn_{1-x}Mg_xO$ samples were exhibited in **Figure 2**a–c.

Table 1. The concentration-dependence of lattice parameters, cell volumes, microstrain, dislocation density, locality of the atoms and their displacement, bond length, and band gap in $Zn_{1-x}Mg_xO$ structures.

	ZnO	$Zn_{0.99}Mg_{0.01}O$	$Zn_{0.98}Mg_{0.02}O$	$Zn_{0.97}Mg_{0.03}O$	$Zn_{0.96}Mg_{0.04}O$	$Zn_{0.95}Mg_{0.05}O$
a [Å]	3.251	3.25182	3.25180	3.25195	3.25217	3.25223
c [Å]	5.21	5.21020	5.21021	5.21019	5.21015	5.21011
c/a	1.601	1.602	1.602	1.602	1.602	1.602
Volume,V[$Å^3$]	47.667	47.7227	47.7223	47.7265	47.7325	47.734
D [nm]	48.12	35.51	33.61	33.20	34.30	29.26
$\mathcal{E}$	0.00072	0.00098	0.00103	0.00104	0.00102	0.00119
δ*10^{14}	0.000431	0.000793	0.000885	0.000907	0.00085	0.001168
u	0.37988	0.37984	0.37984	0.37985	0.37987	0.37988
L [nm]	1.9784	1.97906	1.97905	1.97911	1.97920	1.97922
E_g [eV]	3.199	3.223	3.226	3.239	3.245	3.247

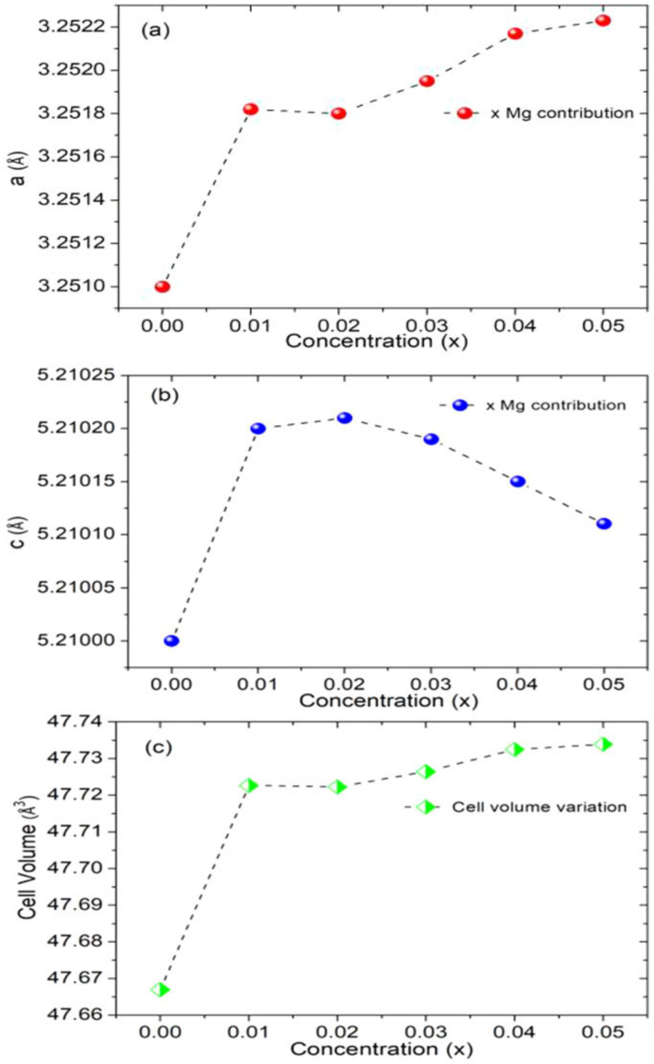

Figure 2. The concentration-dependent lattice parameters and the cell volume variations in $Zn_{1-x}Mg_xO$ samples.

The increment range was observed in in-plane lattice parameter (a) by increasing Mg amount in the samples between 0.02 and 0.05 dopant rate in which a continuous decrease was observed for out-of-plane lattice parameters in Figure 2a,b. This behavior is an indication of horizontal expansion in cell volume by means of increasing the amount of Mg concentration in the samples. The cell volume variation was observed in all Mg contribution steps by partially replacing Mg with Zn in the structures. The increment of Mg in the samples revealed an increment in the cell volume after the concentration rate of $x = 0.02$ in **Figure 2**c. This increment in the cell volume is attributed to a relaxation in the chemical pressure.

In a structure, both doping ratio and annealing temperature are the two main reasons affecting microstrain (ε) as shown in Table 1. The dopant ratio of $x = 0.03$ is the maximum limit point for ε-value and after that the ε-values present a fluctuation with increment Mg amount in the structure. As seen in Table 1, the fluctuations in the strain values may reveal many physical defects and dislocations in the host lattice structure. Therefore, dislocation density (δ) describing the amount of defect in the sample was also studied. As shown in Table 1, the nanorod size exhibits the lowest value with maximum ($x = 0.05$) Mg concentration and δ-value in that concentration is maximum due to the inverse proportion expression between δ- and D-values.[22]

The locality of the atoms and their displacements (u parameters) were calculated and revealed an ignorable increase in $Zn_{1-x}Mg_xO$ samples. The Zn-O bond lengths (L parameters) presented a small increment after the concentration rate of $x = 0.02$. The increasing dopant rate in Mg elements in the pure ZnO structure might be the reason behind Zn-O bond length increments. The detailed calculations of ε, δ, D, u, and L parameters were depicted in ref. [22].

The pure ZnO nanorods have been characterized by Scanning Electron Microscopy (SEM). **Figure 3**a,b shows the SEM picture of ZnO nanorods. It can be seen from these figures that nanorods consist of microrods with almost perfect hexagonal cross section. The whole nanorods are surprisingly divided into two groups with respect to rod sizes. It means that there are no

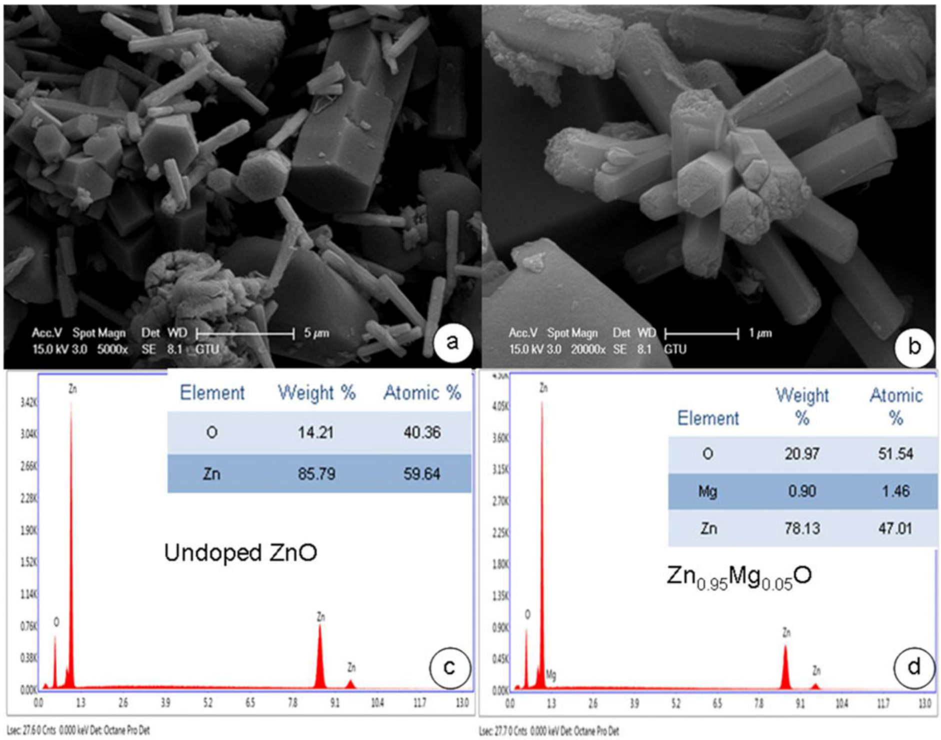

Element	Weight %	Atomic %
O	14.21	40.36
Zn	85.79	59.64

Element	Weight %	Atomic %
O	20.97	51.54
Mg	0.90	1.46
Zn	78.13	47.01

Figure 3. The SEM images a) at low magnification b) at high magnification, and the EDS results for c) pure ZnO and d) $Zn_{0.95}Mg_{0.05}O$ nanorods.

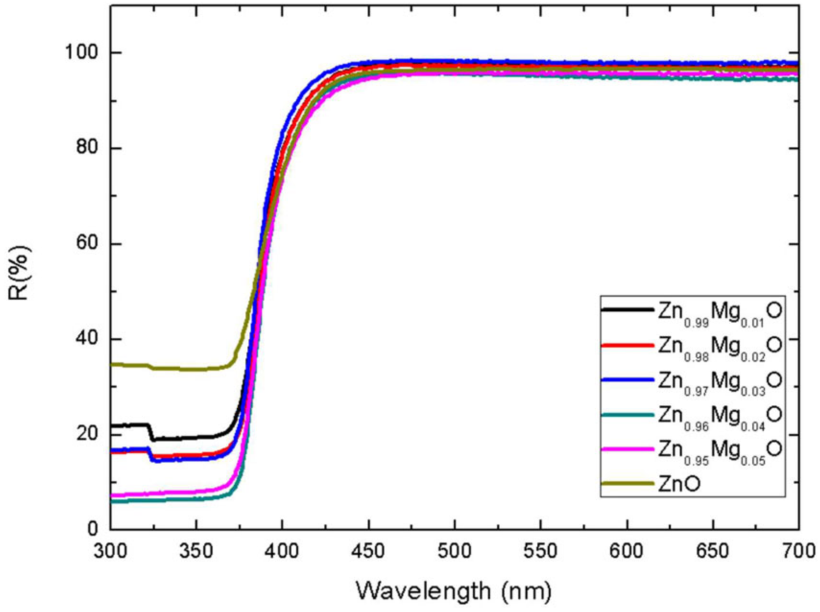

Figure 4. The reflectance spectra of the $Zn_{1-x}Mg_xO$ ($x = 0.0$, 0.01, 0.02, 0.03, 0.04, and 0.05) nanorods.

continuous size distributions. The sizes of larger and smaller roads are quite different from each other as well. The geometric dimensions of rods in one group are at least 5 times larger than those of structures in the other group. All peaks belong to the Zn and O elemental contributions in **Figure 3**c. The atomic ratio of each element was also defined for pure ZnO compositions as seen in the insets of Figure 3c.

3.2. Optical Analysis

The reflectance spectra of $Zn_{1-x}Mg_xO$ ($x = 0.0$, 0.01, 0.02, 0.03, 0.04, and 0.05) nanorods obtained by UV–VIS diffuse reflectance measurements in the range 300–700 nm wavelength is shown in **Figure 4**. It is seen that the reflectance intensities of the samples are around 95 %.

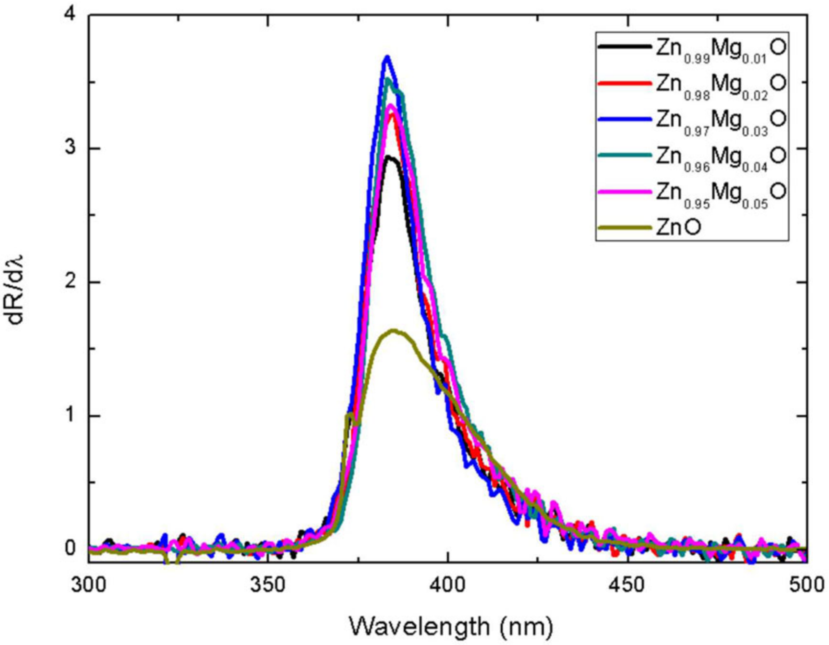

Figure 5. The plots of dR/dλ as a function of wavelength λ for the $Zn_{1-x}Mg_xO$ ($x = 0.0$, 0.01, 0.02, 0.03, 0.04, and 0.05) nanorods.

The optical band gap (E_g) was obtained by plugging the wavelength values of the maximum peaks (λ_{max}) into the following equation:

$$E_g = \frac{hc}{\lambda_{max}} \tag{2}$$

where h is the Planck's constant and c is the speed of light[23] and its graph is obtained by plotting dR/dλ versus λ as shown in **Figure 5**. The obtained E_g-values of $Zn_{1-x}Mg_xO$ ($x = 0.0$, 0.01, 0.02, 0.03, 0.04, 0.05) nanorods are 3.199, 3.223, 3.226, 3.239, 3.245 and 3.247 eV, respectively. It is concluded from Figure 5 that the E_g-values increase with increasing amount of Mg elements in the structure.

3.3. Magnetic Analysis

The ESR spectra of $Zn_{0.95}Mg_{0.05}O$ nanorods were recorded by using Bruker EMX X-band spectrometer (9.8 GHz) with about 20 mW microwave power and 100 kHz magnetic field modulation at room temperature to identify and study the defects in Mg doped ZnO nanorods. The static magnetic field was altered in the range 0–16 000 G. The field derivative of microwave power absorption (dW/dH1) was registered as a function of the applied magnetic field.

These measurements showed that only a single strong peak was observed in these ranges. Furthermore, the distances between the lines were similar. ESR spectrum is dominated by a strong peak at around 3475 G as shown in **Figure 6**. ESR measurements were performed and analyzed using g-factor and the concentration dependence of the peak to peak line-widths ΔH_W, which is defined as the width between points of maximum and minimum of the first derivative of the ESR line. The g-value was calculated, as 2.0148 by resonance equation ($hv = g\beta H$) and line-widths ΔH_W were determined as 11.7 G from the experimental spectra.

In ZnO materials, the ESR line with g = 1.96 (with the components $g_{||} = 1.957$and $g_{\perp} = 1.955$) is usually observed, which is understood as the result of conduction electrons at the surface center of ZnO particles and donor centers in powder Arda et al.[24] Moreover, an ESR signal with g-value 1.995 showing singly ionized oxygen vacancies and with g-values from 2.003 to 2.019 indicating singly ionized zinc vacancy both were observed in Taylor[25] and Galland.[26] In our calculations, it is found that the g-value was greater than 2 which may be due to the Zn vacancy in the structure and this indicated a ferromagnetic behavior of the $Zn_{0.95}Mg_{0.05}O$ nanorods.

4. Conclusion

We observed the structural, magnetic, and optical properties of Mg-doped ZnO nanorods synthesized by the hydrothermal method using varying x-values from 0.0 to 0.05 with 0.01 step increment. XRD and Rietveld refinement analysis exhibited single phase samples, so we conclude that hydrothermal method is one of the convenient methods to obtain single phase for $Zn_{1-x}Mg_xO$ compositions.

Decrease and increase tendencies were observed in (a) and (c) lattice parameters with increasing Mg contribution in the structures. In the cell volume, an increase and saturation were observed by doping more Mg elements to undoped ZnO. The dopant ratio of $x = 0.03$ was the maximum limit point for ε-value

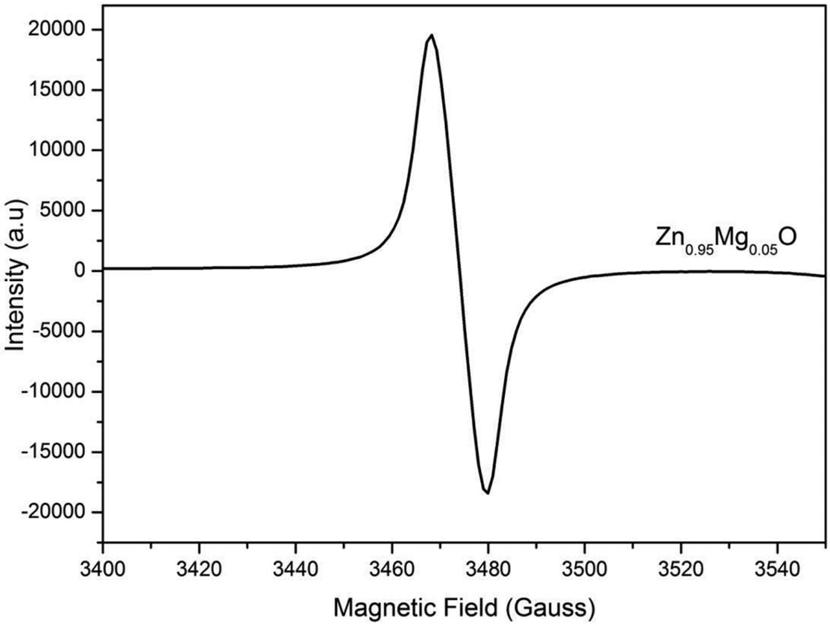

Figure 6. ESR spectrum of $Zn_{0.95}Mg_{0.05}O$ at room temperature.

and after that the ε-values presented a fluctuation with increment Mg amount in the structure. A slight ignorable variation in u and L parameters of $Zn_{1-x}Mg_xO$ samples were observed. The grain size of $Zn_{1-x}Mg_xO$ compositions was observed between 29.26 and 35.51 nm by using the hydrothermal method. The optical band gap energies of the samples revealed that the E_g-values increased with increasing amount of Mg elements in the structure. The optical transmittance of ZnMgO nanorods was determined over 95%. The values of optical band gap showed an increment from 3.199 to 3.247 eV for the concentration of Mg $x = 0.0$ - 0.05 with an increment of 0.01. Finding the g-value greater than 2 can be explained as the Zn vacancy in the structure and this indicates a ferromagnetic behavior of the $Zn_{0.95}Mg_{0.05}O$ nanorods.

Acknowledgements

This research was supported by the Abant İzzet Baysal University Scientific Research Projects under the Project No: BAP- 2015.03.03.925 and the Research Fund of Bahcesehir University (BAU-BAP.2018.02.16).

Conflict of Interest

The authors declare no conflict of interest.

Keywords

hydrothermal method, magnetic properties, nanorod, optical properties, zinc oxide

Received: October 11, 2018
Revised: December 12, 2018

[1] U. Ozgur, I. A. Ya, C. Liu, A. Teke, M. A. Reshchikov, S. Dogan, V. Avrutin, S. J. Cho, H. Morkoc, *J. Appl. Phys.* **2005**, *98*, 041301.
[2] Z. K. Heiba, L. Arda, *Cryst. Res. Technol.* **2009**, *44*, 845, and the references therein.
[3] Z. K. Heiba, L. Arda, M. B. Mohammed, Y. M. Nasser, N. Dogan, *J. Supercond. Novel Magn.* **2013**, *26*, 3487.
[4] N. Sinha, G. Ray, S. Bhandari, S. Godara, B. Kumar, *Ceram. Int.* **2014**, *40*, 12337.
[5] S. B. Woodley, A. A. Sokol, C. Richard A. Catlow, A. A. Al-Sunaidi, S. M. Woodley, *J. Phys. Chem. C* **2013**, *117*, 27127.
[6] E. Asikuzun, O. Ozturk, L. Arda, D. Akcan, S. D. Senol, C. Terzioglu, *J. Mater. Sci: Mater. Electron.* **2015**, *26*, 8147.
[7] M. Tosun, S. Ataoglu, L. Arda, O. Ozturk, E. Asikuzun, D. Akcan, O. Cakiroglu, *Mater. Sci. Eng.: A* **2014**, *590*, 416.
[8] L. Arda, *J. Magn. Magn. Mater.* **2019**, *475*, 493.
[9] M.-H. Hsu, C.-J. Chang, *J. Hazard. Mater.* **2014**, *278*, 444.
[10] S. M. Lukas, L. M. D. Judith, *Mater. Today* **2007**, *10*, 40.
[11] A. Ohtomo, M. Kawasaki, T. Koida, K. Masubuchi, H. Koinuma, *Appl. Phys. Lett.* **1998**, *72*, 2466.
[12] N. Guo, X. Q. Wei, R. R. Zhao, X. J. Xu, *Appl. Surf. Sci.* **2014**, *317*, 400.
[13] A. H. Qusay, A. Nasera, J. Zhoua, H. Wang, G. Liu, L. Wang, *Optical Mater* **2015**, *46*, 22.
[14] Y. Wang, X. Zhao, L. Duan, F. Wang, H. Niu, W. Guo, A. Ali, *Mater. Sci. Semicond. Process.* **2015**, *29*, 372.
[15] X. Gu, B. Wang, Y. Zhao, Y. Qiang, *J. Mater Sci: Mater. Electron* **2013**, *24*, 884.
[16] N. Kilinç, L. Arda, S. Öztürk, Z. Z. Öztürk, *Cryst. Res. Technol.* **2010**, *45*, 529.
[17] J. Li, H. Zhuang, J. Wang, P. Xu, *Phys. Status Solidi A* **2011**, *208*, 136.
[18] S. D. Senol, O. Ozturk, C. Terzioğlu, *Ceram. Int.* **2015**, *41*, 11194.
[19] J. Yang, Y. Wang, J. Kong, M. Yu, H. Jin, *J. Alloys Compd.* **2016**, *657*, 261.

[20] S. Baruah, J. Dutta, *Sci. Technol. Adv. Mater.* **2009**, *10*, 013001.

[21] A. L. Patterson, *Phys. Rev.* **1939**, *56*, 978.

[22] C. Boyraz, N. Dogan, L. Arda, *Ceram. Int.* **2017**, *43*, 15986.

[23] A. F. da Silva, N. Veissid, C. Y. An, I. Pepe, N. B. de Oliveira, A. V. B. da Silva, *Appl. Phys. Lett.* **1996**, *69*, 1930.

[24] L. Arda, M. Açıkgöz, N. Doğan, D. Akcan, O. Çakıroğlu, *J. Supercond. Novel Magn.* **2014**, *27*, 799.

[25] A. L. Taylor, G. Filipovich, G. K. Lindeberg, *Solid State Commun.* **1970**, *8*, 1359.

[26] D. Galland, A. Herve, *Phys. Lett. A* **1970**, *33*, 1.